SEAFaIR: a generalised impulse-response model for climate uncertainty and future scenario exploration, integrated assessment, and teaching

Nicholas J. Leach[1⋆]

Stuart Jenkins[1]

John Lynch[1]

Michelle Cain[1,2]

Bill Wu[1]

Junichi Tsutsui[3]

Christopher Smith[4]

Zebedee Nicholls[5]

Myles R. Allen[1,2]

[1]Department of Physics, Atmospheric Oceanic and Planetary Physics, University of Oxford, United Kingdom.

[2]Environmental Change Institute, University of Oxford, Oxford, UK.

[3]Environmental Science Laboratory, Central Research Institute of Electric Power Industry, Abiko-shi, Japan.

[4]School of Earth and Environment, University of Leeds, Leeds, UK.

[5]Australian–German Climate and Energy College, University of Melbourne, Australia

⋆contact email: `Nicholas.leach@stx.ox.ac.uk`

Abstract

Here we present a new simple climate model for use in probabilistic future climate and scenario exploration, integrated assessment, policy and teaching. This model is based on a set of only six equations, which correspond to the AR5-IR model plus one additional equation which includes physically-motivated state-dependent feedbacks on the response timescales of each modelled gas

cycle, allowing for a much more accurate representation. These six equations are simple and transparent enough to be easily understood and used in teaching, but flexible enough to be able to accurately (with respect to the observational record) model key climate variables such as well-mixed greenhouse gas (GHG) concentrations and atmospheric lifetimes, effective radiative forcing, and forced temperature anomaly. We describe the assumptions and methods used in selecting the default parameters, but emphasize that other methods would be equally valid, and could lead to alternative model output. The tunable nature of the model lends it to use as an emulator of high complexity Earth System Models, such as those participating in CMIP6, and allows the properties of these complex models to be investigated compared more simply. The model design is such that it can be written in tabular data analysis software, such as Excel, increasing the potential user base of the model considerably. While much of our study is verification of the model, and therefore repeating previous experiments, we calculate the inital pulse-adjustment timescale (the delay between a pulse emission of a GHG and the following peak in warming) for CO_2, CH_4 and N_2O at the present-day, obtaining values of 11.9 [6.9 , >100] , 6.9 [5.1 , 8.4] and 17.0 [11.8 , 23.9] years respectively. These values have important implications for future mitigation efforts and potential trade-offs between reductions of these three GHGs.

1 Introduction

Earth System Models (ESMs) are vital tools for providing insight into the drivers behind Earths climate system, as well as predicting impacts of future emissions. Large scale multi-model studies, such as the Coupled Model Intercomparison Project (CMIP), have been used in many reports to produce projections of what the future climate may look like based on a range of different emissions scenarios and associated socio-economic narratives provided by Integrated Assessment Models (IAMs). In addition to simulating both the past and possible future climates, these CMIPs extensively use theoretical experiments to try to constrain some of the key properties of the climate system, such as the equilibrium climate sensitivity [ECS, Collins et al. (2013)], or the transient climate response to cumulative carbon emissions [TCRE, Allen et al. (2009)]. While ESMs are integral to our current best understanding of the how the climate system responds to GHG emissions, and provide the current best predictions for what a future world might look like, they are so computationally expensive that we are only able to run a limited set of experiments during a CMIP. This constraint on the quantity of experiments and scenarios

able to be simulated necessitates the use of simpler emulators to provide probabilistic assessments and explore additional experiments and scenarios. These emulators are often referred to as simple climate models (SCMs). In general, they are able to simulate the globally averaged emission $\rightarrow$ concentration $\rightarrow$ radiative forcing $\rightarrow$ temperature response pathway, and can be tuned to emulate an individual ESM (or multi-model-mean). In terms of complexity, SCMs are considerably lighter than ESMs, both in terms of the runtime (most SCMs can run thousands of years of simulation per minute on an "average" personal computer, whereas ESMs take several hours to run a single year on a supercomputer), and the number of lines of code (SCMs tend to be composed of the order of thousands, whereas ESMs are of the order of millions of lines).

Several simple climate models are available, such as the two used in the Intergovernmental Panel on Climate Change (IPCC) Special Report on 1.5°C warming (IPCC, 2018, SR15): FaIR v1.3 and MAGICC6. However, while these models are "simple" in comparison to the ESMs they emulate, they are often still not so simple as to allow new users to quickly and easily understand the equations and processes behind their calculations. This learning curve behind the use of these simple models reduces their usability, and has meant that different research groups tend to use the model they are most familiar with. This has led to a number of different simple climate models being used in single reports for identical tasks, reducing the overall consistency of the work. We believe one key step towards a transparent and coherent process in reports such as SR15 is the use of a single SCM between working groups, and would allow results to be directly comparable throughout. Such a model would be a "lowest common denominator" model within these reports.

In this paper, we introduce a simple, transparent, and flexible climate model based on the Finite amplitude Impulse Response (FaIR) model v1.0 (Millar et al., 2017) that uses four equations to model the atmospheric cycles and corresponding effective radiative forcing (ERF) impact of three major greenhouse gases, and a further two to emulate the climate system's thermal response to changes in ERF; these are outlined in figure 1. As such, we have chosen to call the model SEAFaIR (Six Equation Analytical FaIR). Despite their simplicity, these equations do still represent physical process and the model is therefore not an entirely abstracted emulator with no basis in the real world. We describe

the methods behind selecting a default parameter set and associated uncertainties for the model using some constraints from more complex models and existing literature, but ultimately chosen to accurately represent historical observations. We demonstrate that this parameter set can closely replicate inferred properties of the climate system in both historical observations and more complex models. We compare SEAFaIRs response with other widely used simple climate models for a subset of the Shared Socioeconomic Pathways ,(Riahi et al., 2017, SSPs), all using their respective default parameter sets. Previous work (Joos et al., 2013; Tsutsui, 2017) indicates that the model parameters can be adjusted to emulate the behaviour of ESMs, suggesting that SEAFaIR could act as a probabilistic emulator for individual CMIP6 ESMs, something we aim to demonstrate when sufficient CMIP6 output is available.

SEAFaIR is sufficiently simple as to be able to be used (and crucially understood) in undergraduate and high-school teaching of climate change, and can illustrate some key properties of the climate system such as the very different warming impacts of different GHGs, or the widely discussed equilibrium climate sensitivity. To allow students and other users unfamilliar with scientific programming languages (such as SEAFaIR's native language, python) access to the model, we also provide a version of SEAFaIR written in Excel. We hope that this may open exploration of the climate system to a large group of potential users who do not have the expertise to run presently-available available SCMs. The simplicity of SEAFaIR additionally means that although we provide model code, users do not need to rely on this, and would be able to relatively quickly re-create it in whatever language they are familiar with, and whatever format fits their intended usage. This increases the potential of SEAFaIR for use in integrated assessment, as instead of having to adapt existing code to run within an existing architecture, new code for this model could be written in exactly the format and structure required.

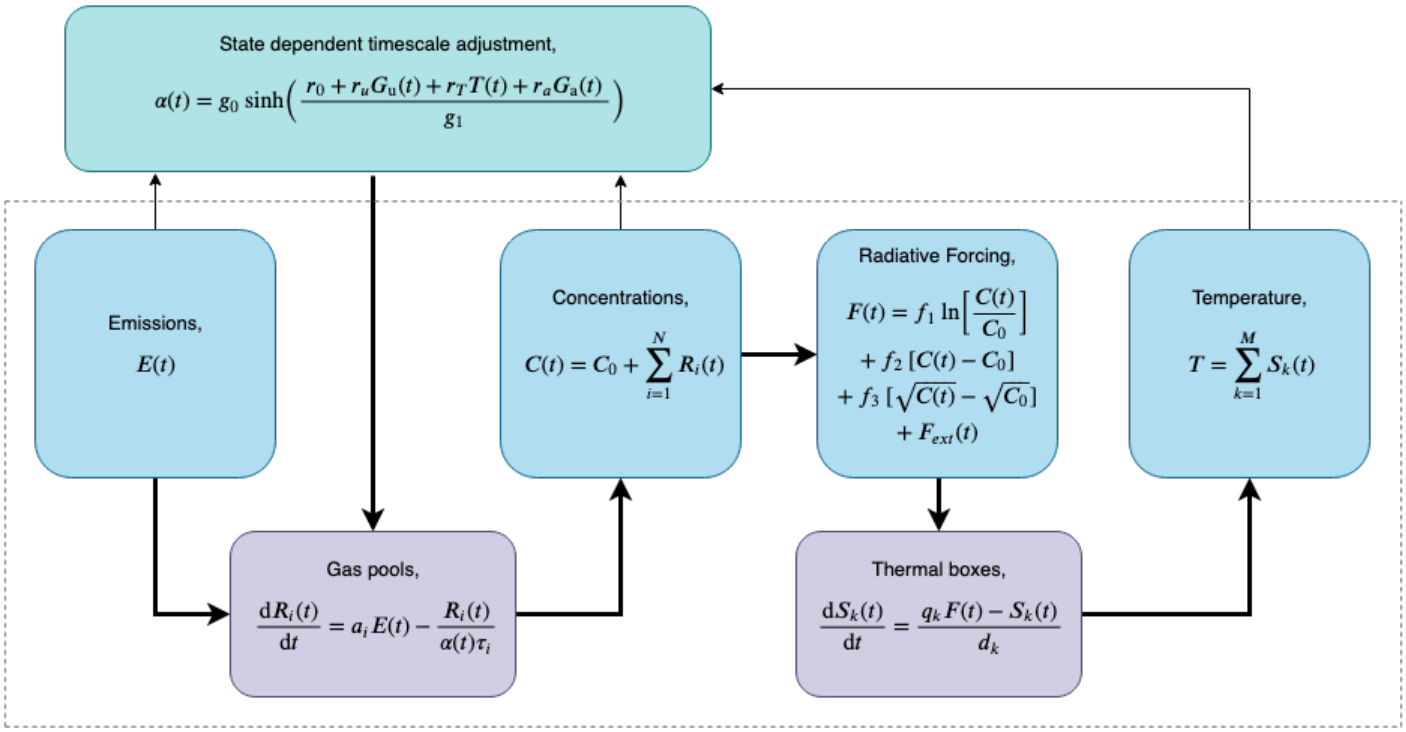

Figure 1: Schematic showing the full model structure and equations used. Model steps take place from left to right, with thick arrows indicating the flow of model steps that occur during timestep t, and thin arrows indicating steps that occur in between timesteps t and $t + dt$. Equations are described in full below. The dashed grey line indicates the components identical to AR5-IR (Myhre et al., 2013).

2 Emissions to concentrations

Model description

SEAFaIR models the relationship between emissions and atmospheric concentrations of a gas species (the gas cycle) with three equations:

$$\frac{\mathrm{d}R_i(t)}{\mathrm{d}t} = a_i E(t) - \frac{R_i(t)}{\alpha\tau_i}, \tag{1}$$

$$C(t) = C_0 + \sum_{i=1}^{n} R_i(t) \quad \text{and} \tag{2}$$

$$\alpha(t) = g_0 \cdot \sinh\Big(\frac{r_0 + r_u G_u(t) + r_T T(t) + r_a G_a(t)}{g_1}\Big); \tag{3}$$

$$\text{where} \quad g_1 = \sum_{i=1}^{4} a_i\tau_i\big[1 - \big(1 + h/\tau_i\big)\mathrm{e}^{-h/\tau_i}\big]$$

$$\text{and} \quad g_0 = \Big[\sinh\Big(\frac{\sum_{i=0}^{3} a_i\tau_i[1 - \mathrm{e}^{-h/\tau_i}]}{g_1}\Big)\Big]^{-1}.$$

Equations 1 and 2 describe a gas cycle with an atmospheric burden above the pre-industrial concentration, C_0, formed of n pools: each pool corresponds to a different sink from the atmosphere. Each pool, R_i, has an uptake fraction a_i and decay timescale τ_i, which is multiplicatively adjusted by a state dependent factor, α. At each timestep, time t, α is computed, and then the pool concentrations are updated and summed to determine the new atmospheric burden. α provides feedbacks to the gas lifetimes based on the current timestep levels of accumulated gas, temperature, and atmospheric gas burden, encapsulated by the r coefficients. The form of α, 3, is an analytic approximation to the numerical solution of the 100-year integrated Impulse Response Function (iIRF100) from equations 7 and 8 in Millar et al. (2017). We include possible state dependencies on the cumulative carbon uptake mass, G_u, the temperature, T, and an additional term not in FaIR v1.3 dependent on $G_a(t)$, the atmospheric mass burden, motivated by the sensitivities of the CH_4 and N_2O lifetimes to their own abundances as predicted by atmospheric chemistry and simulated in chemical transport models (CTMs) (Holmes et al., 2013; Prather et al., 2015). g_0 and g_1 set the value and gradient of our analytic approximation equal to the numerical solution at $\alpha = 1$. We discuss the suitability of this analytic form in the Supplementary Information and compare it to the numerical solution used in FaIR v1.3 (Smith et al., 2017). While we do not include any lifetime feedbacks beyond those described above to avoid having to specify ad-

ditional exogenous variables, such as NOx feedback on the CH_4 lifetime, these could theoretically be incorporated in the same framework by adding r coefficients to the model.

Observationally consistent parameter selection

Here we discuss default parameter choices for the three greenhouse gases (GHGs) that have contributed the most to global warming since pre-industrial times: carbon dioxide (CO_2), methane (CH_4) and nitrous oxide (N_2O). The CO_2 gas cycle is highly similar to those in FaIR v1.0 (Millar et al., 2017) and FaIR v1.3 (Smith et al., 2017): a four carbon pool cycle with a decay timescale dependence on G_u and T. The CH_4 gas cycle has a single pool, with lifetime state dependencies on T and G_a. While in reality, CH_4 has several sinks (tropospheric OH, tropospheric Cl, stratospheric reactions and soil uptake) and a lifetime dependent on many more variables (Holmes et al., 2013), we find that SEAFaIR is sufficient for reproducing observed emission to concentration pathways. The N_2O gas cycle has a single pool and a lifetime dependent only on G_a.

For CO_2 we keep values of a_i and τ_i identical to those in FaIR v1.0 and v1.3 (Millar et al., 2017; Smith et al., 2017), originally from Myhre et al. (2013). r_0, r_u and r_T are tuned to reproduce present day concentrations – from the CMIP6 historical concentrations dataset, extended to 2017 with up-to-date measurements from NOAA (Meinshausen et al., 2017; Battle et al., 1996; Butler et al., 1999) – when SEAFaIR is spun up from pre-industrial with bottom-up emission estimates from the Global Carbon Project (Quéré et al., 2018) and run with a prescribed temperature pathway of attributable warming to the present day [calculated as described in Haustein et al. (2017) using best-estimate forcings based on Forster et al. (2013) and the mean of four temperature datasets (Vose et al., 2012; Cowtan and Way, 2014; Lenssen et al., 2019; Morice et al., 2011)], fixing the ratio of r_u and r_T to the FaIR v1.0 and v1.3 default. Uncertainties in r_0, r_u and r_T are taken from Millar et al. (2017).

The CH_4 gas cycle only has a single pool, so a_i is zero except for $i = 1$. We set τ_1 to the present-day lifetime found in Holmes et al. (2013). We fit r_T and r_a to the sensitivities of the CH_4 lifetime to tropospheric air temperature, tropospheric water vapour and CH_4 abundance in Holmes et al. (2013) by linearising SEAFaIR and the parametric model in Holmes et al. about 2010 variable values. We find

that a global mean temperature dependence is sufficient to reproduce the sensitivities to both tropospheric air temperature and water vapour due to the close thermodynamic relationship between these quantities. We then fit the specified pre-industrial concentration and r_0 in an identical model run to the CO_2 parameter fitting procedure, but using bottom-up emission estimates from PRIMAP-histTP (Gütschow et al., 2016). While the parametric model in Holmes et al. includes lifetime sensitivities to eight other atmospheric variables such as anthropogenic NOx emissions, many of these have a small effect and all are scenario-dependent, requiring additional exogenous variables to be specified. Since we wish each gas cycle model to be independent we do not include any more state dependencies in addition to those described above. Uncertainties in τ_1, r_T and r_a are derived from the uncertainties given in Holmes et al. (2013). We recommend that when using a Transient Climate Reponse (TCR) thermal parameter value that differs from the central estimate of 1.58K, both the CO_2 and CH_4 r_T parameter values be scaled to match the ratio of the chosen TCR to the central estimate.

The N_2O gas cycle only has a single pool, so a_i is zero except for $i = 1$. We set τ_1 to the present-day lifetime found in Prather et al. (2015). We fit r_a to the sensitivity of the N_2O lifetime to its own burden found in Prather et al. (2015) by linearising SEAFaIR and the parametric model in Prather et al. about 2010 variable values. We then fit the specified pre-industrial concentration and r_0 as for CH_4. All other variables that affect the N_2O lifetime in Prather et al. are discarded to keep the gas cycle model independent as with CH_4. Uncertainties in τ_1 and r_a are derived from the uncertainties given in Prather et al. (2015).

The resulting tuned default parameters are given below, alongside their values in FaIR v1.0 and v1.3. Note that FaIR v1.3 has effective parameter values of r_u, r_T, $r_a = 0$ and a value of r_0 set such that $\alpha = 1$, and that FaIR v1.0 does not include CH_4 or N_2O. We emphasize that many choices have been made in selecting these parameters and different choices would lead to potentially quite different parameter values. One example of this is given in parentheses, in which we fit the CH_4 r_0 parameter by tuning inverse emissions from SEAFaIR to the best-estimate top-down anthropogenic emission estimate in the recent Global Methane Budget (Saunois et al., 2019), while setting the pre-industrial concentration to the 1500-1800 mean of 720 ppb from Meinshausen et al. (2017).

Table 1: Default parameter values for the gas cycle components in different versions of FaIR. Where relevant, uncertainties for SEAFaIR are included as the 1-σ range and are assumed to be normally distributed.

Parameter	SEAFaIR			FaIR v1.3			FaIR v1.0		
	CO_2	CH_4	N_2O	CO_2	CH_4	N_2O	CO_2	CH_4	N_2O
a_1	0.2173	1	1	0.2173	1	1	0.2173	-	-
a_2	0.2240	0	0	0.2240	0	0	0.2240	-	-
a_3	0.2824	0	0	0.2824	0	0	0.2824	-	-
a_4	0.2763	0	0	0.2763	0	0	0.2763	-	-
τ_1	1000000	$9.15 \pm 10\%$	$116 \pm 8\%$	1000000	9.3	121	1000000	-	-
τ_2	394.4	-	-	394.4	-	-	394.4	-	-
τ_3	36.54	-	-	36.54	-	-	36.54	-	-
τ_4	4.304	-	-	4.304	-	-	4.304	-	-
r_0	$28.63 \pm 8\%$	9.079 (8.445)	67.84	35.0	-	-	32.4	-	-
r_u	$0.01977 \pm 8\%$	0	0	0.019	-	-	0.019	-	-
r_T	$4.334 \pm 8\%$	$-0.2872 \pm 15\%$	0	4.165	-	-	4.165	-	-
r_a	0	$0.0003434 \pm 13\%$	$-0.0009993 \pm 16\%$	0	-	-	0	-	-
C_0	278	733.8 (720.0)	271.26	278	-	-	278	-	-
$E2C$	0.4690	0.3517	0.2010	0.4690	0.3517	0.2010	0.4690	-	-

Specification of natural emissions

One key difference between SEAFaIR and FaIR v1.3 is the treatment of natural emissions of CH_4 and N_2O. FaIR v1.3 requires a quantity of natural emissions to be specified for these gases, which is also the case for the widely used simple climate model MAGICC (Meinshausen et al., 2011a). Figure 2 in Smith et al. (2017) illustrates the time-dependent pathway of natural emissions required to reproduce the historical Representative Concentration Pathway (RCP) concentrations when the corresponding emission timeseries (Meinshausen et al., 2011b) are run through FaIR v1.3. These natural emission timeseries vary significantly over the recent past: CH_4 drops from 209Mt in 1765 to 139Mt in 1900 then rises to its fixed future (2005 onwards) value of 191Mt, at which it is fixed following; and N_2O remains relatively constant around 11Mt before dropping sharply to its fixed future value of 9Mt around 1950. This procedure of "balancing the emissions budget" to reproduce observed historical concentrations is also utilised in MAGICC (Meinshausen et al., 2011a). This is required since the RCP database emission series were created in parellel to the concentration pathways used in CMIP5 using Integrated Assessment Models Moss et al. (2010); resulting in inconsistent emission and concentraiton data. There is little evidence for the high interdecadal trends of these natural emission pathways: Arora et al. (2018) finds the total change in natural CH_4 fluxes within CLASS-CTEM between the 1850s and 2000-2008

is +17Mt, and other studies assume that there have been no significant changes (Holmes et al., 2013; Prather et al., 2012). Due to the uncertainties associated with natural emissions of CH_4 and N_2O (Turner et al., 2019; Davidson and Kanter, 2014), we have chosen to effectively fix our natural emissions by specifying a pre-industrial concentration over which anthropogenic emissions sources increase the atmospheric concentration burden, as in the CO_2 gas cycle in all FaIR versions, and tune our gas cycle parameters to bottom-up emissions (Gütschow et al., 2016; Quéré et al., 2018) and observed concentrations Meinshausen et al. (2017) entirely independently of the RCPs. For comparison with FaIR v1.3, Figure 1 in the Supplementary Information shows the residual of emissions required to reproduce the RCP historical concentrations in SEAFaIR and the historical RCP emissions dataset. This is closely related to Figure 2 in Smith et al. (2017), indicating that while SEAFaIR and v1.3 take different approaches to natural emissions, the gas cycle models used by each are similar.

Emission-driven historical simulations

Here we run SEAFaIR with bottom-up emissions timeseries from the Global Carbon Project for CO_2 (Quéré et al., 2018) and PRIMAP-histTP (Gütschow et al., 2016) for CH_4 and N_2O. All other forcings are best-estimates from Forster et al. (2013). Figure 1 shows the gas concentrations as simulated in SEAFaIR with default parameters and uncertainties as described in both the gas cycle and thermal response parameters, plotted alongside obesrved concentrations from the CMIP6 historical dataset Meinshausen et al. (2017). Inset axes show the driving emission series used. We see that in general, SEAFaIR does well at matching the observed values, with the largest difference occurring for pre-1950 concentrations of N_2O. However, rather than this being a fundamental issue with the model, it is clear that the emission timeseries used is not compatible with the observed concentrations, as while concentration observations start increasing pre-1900, emissions only begin to increase around 1940. This discrepancy has occurred in other N_2O modelling studies using different methods and data sources (Saikawa et al., 2014). This is an issue of ongoing research (Tian et al., 2018), and it is possible that future work may provide a firm reason for this descrepancy, allowing us to adjust SEAFaIR parameters accordingly. Crucially, the model does match the trend in observed concentrations over the recent period, where we would expect the emission estimates to be most accurate. We find that the pre-industrial lifetimes of CH_4 and N_2O are 9.05 ± 0.4 and 119.9 ± 0.2 years; pre-industrial natural emissions are $230 \pm 6 MtCH_4$ and

11.3 ± 0.2MtN$_2$O-N$_2$; and present-day (2016) lifetimes are 10.1 ± 0.9 and 118.5 ± 0.5 years respectively. These quantities are within the assessed ranges found in more specific studies (Prather et al., 2012, 2015; Holmes et al., 2013; Kirschke et al., 2013; Davidson and Kanter, 2014; Arora et al., 2018).

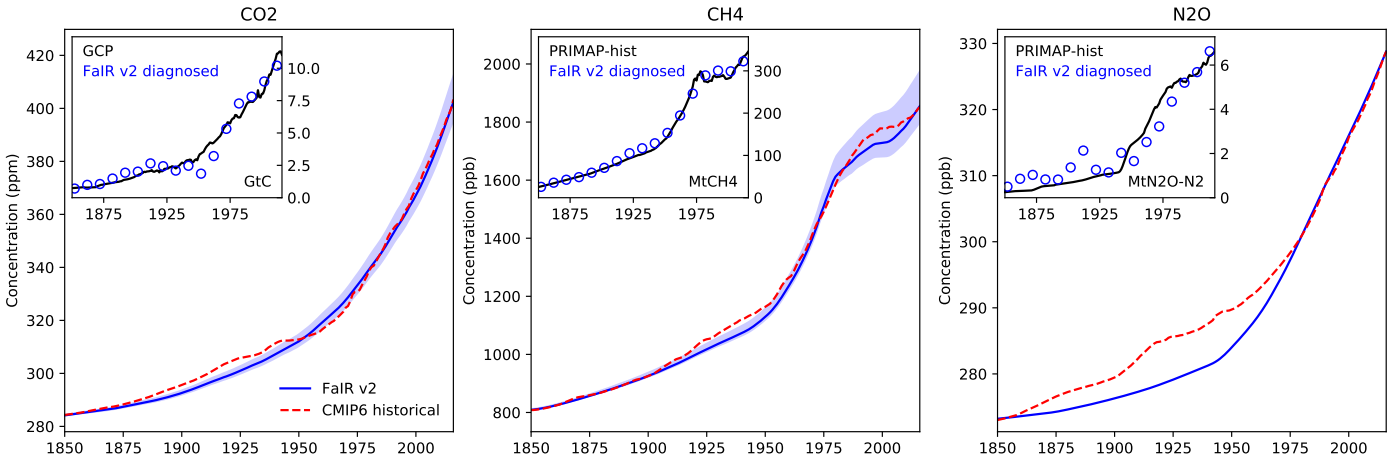

Figure 2: Historical simulations with SEAFaIR. Blue solid lines show SEAFaIR default concentration response to bottom-up emission data, and light blue plume shows 5-95% range. Dotted red lines show concentrations from Meinshausen et al.. Inset axes show corresponding bottom-up emission data, alongside decadal mean SEAFaIR diagnosed inverse emissions from Meinshausen et al. concentrations.

Other well-mixed GHGs

While here we focus on the three major GHGs, SEAFaIR can also be used to simulate gas cycles for the other 40 well-mixed halogenated GHGs found in the CMIP6 historical concentrations (Meinshausen et al., 2017). A figure depicting SEAFaIR inverse emissions from these concentrations and inverse emission estimates from a more complex atmospheric chemistry model (Cunnold et al., 1994; Rigby et al., 2011) is provided in the Supplementary Information alongside parameter values and a description of the tuning process for these gases. We note that for several gases – HFC-32, HFC-227ea, HFC-245fa, HFC-43-10-mee and C6F14 – SEAFaIR deviates significantly from the RCP database emissions. There is no observational evidence for the RCP pathways in these cases (Vollmer et al., 2011; Ivy et al., 2012; O'doherty et al., 2014).

3 Concentrations to effective radiative forcing

FaIR uses a simple formula to relate atmospheric gas concentrations to effective radiative forcing. This equation, below, includes logarithmic, square-root, and linear terms; motivated by the concentration-forcing relationships in Myhre et al. (2013) of CO_2, CH_4 and N_2O, and all other well-mixed GHGs respectively.

$$F(t) = f_1 \cdot \ln\Big[\frac{C(t)}{C_0}\Big] + f_2 \cdot [C(t) - C_0] + f_3 \cdot [\sqrt{C(t)} - \sqrt{C_0}] + F_{ext}, \tag{4}$$

where the f coefficients are specified parameters, $C(t)$ is the concentration at time t and C_0 is the pre-industrial concentration of the gas species.

Selecting parameters based on Etminan et al. (2016)

SEAFaIR is tuned to match the simple formulae for radiative forcing of CO_2, CH_4 and N_2O given in Etminan et al. (2016). However, while Etminan et al. includes interactions between the three gases, SEAFaIR does not for consistency with our aim to keep the gas species independent of one another. To tune the three f parameters to Etminan, we use the CMIP6 historical concentration dataset (Meinshausen et al., 2017), and first fit them to the simple formula in Etminan et al. with interaction terms discarded. We then add on the present day value of each interaction term to the relevant f parameter (f_1 for CO_2 and f_3 for CH_4 and N_2O). Our fit parameters give an effective radiative forcing under a doubling of CO_2, $F_{2\times CO_2}$ of 3.80 Wm^{-2}. Figure 5 in the Supplementary Information shows the radiative forcings of CO_2, CH_4 and N_2O over the RCP database concentrations as computed using our equation in comparison to the formulae in Etminan et al., both with and without interaction terms. We see that our equation very closely resembles the formulae in Etminan et al., only deviating slightly under the very high concentrations in RCP8.5. Including present-day interaction coefficients improves our equations significantly for CH_4 and N_2O over all the RCPs. Our equation's maximum deviation from Etminan over the RCPs (though it occurs in RCP8.5 for all three gases) is 3%, 2% and 10% for CO_2, CH_4 and N_2O respectively; Figure 6 in the SI shows deviations against gas concentrations from which these values are obtained. These errors are less than the absolute error in the line-by-line calculations performed by Etminan et al.. However, we note here that the relatively larger error in N_2O RF calculated for RCP8.5 is due to the very high CH_4 concentrations reached, arising from increasing coal production throughout

the 21st century, which has been suggested is unrealistic.

CH_4 concentrations also indirectly affect effective radiative forcing through oxidation to stratospheric water vapour and its effect on atmospheric ozone (Noël et al., 2018; Owens et al., 1982; Myhre et al., 2013). As well as the default parameters that do not include these indirect CH_4 forcings, we provide an alternative f_2 parameter value derived from ordinary least squares regression of atmospheric CH_4 burden against best-estimate forcings of tropospheric and stratopsheric ozone, and stratospheric water vapour. The default parameters, alternative CH_4 f_2 are given below, alongside present-day (2018) effective (direct) radiative forcings (ERF) of each gas based on the CMIP5 historical concentration dataset (Meinshausen et al., 2017) and default SEAFaIR pre-industrial concentrations.

Table 2: Default parameter values for the concentration-forcing relationships in SEAFaIR. An alternative CH_4 f_2 parameter value including indirect forcing effects is given in parentheses.

Parameter	CO_2	CH_4	N_2O
f_1	4.991	-0.06002	0.0009852
f_2	0.001801	-0.0001013 (0.0002873)	0.00009272
f_3	-0.02341	0.04944	0.1058
Present-day ERF (Wm^{-2})	2.06	0.626	0.188

4 The thermal response model

The thermal response model is a simple linear step response model (Good et al., 2011). While previous similar models have tended to use two timescales, here we leave the number of response timescales in SEAFaIR general, such that if more are desired, e.g. for a faster response to volcanoes or pulse experiments as in Tsutsui (2017), the user may specify how many to use. The two equations modelling the thermal response are below.

$$\frac{\mathrm{d}S_i(t)}{\mathrm{d}t} = \frac{q_j F(t) - S_i(t)}{d_i} \tag{5}$$

$$\text{and} \quad T(t) = \sum_i^N S_i(t), \tag{6}$$

where S_i represents the temperature anomaly in box i with response timescale d_i at time t, $F(t)$ is the effective radiative forcing, and $T(t)$ is the global mean surface temperature anomaly. As in Millar et al. (2017) and Tsutsui (2017), these equations can be solved analytically to relate q_i and d_i to the Transient Climate Response (TCR) and Equilibrium Climate Sensitivity (ECS) (Collins et al., 2013) as follows:

$$\mathrm{ECS} = F_{2\times\mathrm{CO_2}} \sum_{i}^{N} q_i \tag{7}$$

$$\mathrm{TCR} = F_{2\times\mathrm{CO_2}} \sum_{i}^{N} \left\{ q_i \left(1 - \frac{d_i}{70} \left[1 - e^{-\frac{70}{d_i}} \right] \right) \right\}. \tag{8}$$

When discussing parameters for the two timescale thermal model, we quote TCR and ECS values rather than q parameters since these are the more commonly used quantities.

Selected default parameters

This thermal response model has been previously studied in detail (Geoffroy et al., 2013b,a; Gregory et al., 2015; Smith et al., 2017). Here we adopt the same default thermal response timescales as in FaIR v1.0 and v1.3 (Millar et al., 2017; Smith et al., 2017) from the CMIP5 multi-model-mean found in Geoffroy et al. (2013b). For the TCR and ECS, we adopt the central values from a lognormally distributed TCR with 5-95 percentiles of 1.0 and 2.5 (Collins et al., 2013); and a normally distributed realised warming fraction (the TCR:ECS ratio, RWF) with 5-95 percentiles of 0.45 and 0.75 (Millar et al., 2017). We specify a distribution for the RWF rather than the ECS since the RWF is shown to be more statistically independent of the TCR compared to the ECS (Millar et al., 2015). The central values are TCR = 1.58K and ECS = 2.66K, corresponding to $q_1 = 0.301$ and $q_2 = 0.399$ for our default $d_1 = 239.0$ and $d_2 = 4.10$ timescales. Following Smith et al. (2017) we use gaussian distributions truncated at $\pm 3\sigma$ for the timescales, with $[\mu\ ,\ \sigma] = [239\ ,\ 63]$ and $[4.1\ ,\ 1]$. These distributions as described above are used to generate uncertainty in the thermal response throughout this study.

Confusion arising from the thermal response of simple models

One point of contention within the recent Special Report on 1.5°C warming (IPCC, 2018, SR15) was the difference in apparent response between the two simple models FaIR v1.3 (henceforth FaIR) and

MAGICC6 (MAGICC), with the FaIR response significantly below the MAGICC response in the published model outputs from the IAMC scenarios (Huppmann et al., 2018). Figures 6 and 7 below include the median total forcings and temperature responses in each model to a range of scenarios from the IMAGE 3.0.1 integrated assessment model (IAM). This shows that while the total forcings derived from emissions by each model are relatively similar, with FaIR simulating a slightly wider range (between scenarios) of forcings than MAGICC, the temperature response in FaIR is consistently lower than MAGICC, particularly notable for the high emission SSP5-Baseline scenario. This difference in response is likely due to the default parameter choice in each model, with MAGICC reseponse parameters tuned to output from CMIP3 atmosphere and oceanic general circulation models (AOGCMs) (Meinshausen et al., 2011a), while the response in FaIR (an identical thermal model to that in SEAFaIR) was tuned to constrain modelled response to the observed temperature changes from Cowtan and Way (2014). Here we emphasize that the models themselves are not systematically biased either low or high — it is the parameters used, and how these are selected, that determines the model response. In SEAFaIR we have chosen to use accepted values from the literature for our thermal response parameters as above, which will have a lower default response than both MAGICC and the CMIP3, CMIP5 and CMIP6 AOGCM means, but any user can tune parameters based on what they desire SEAFaIR to emulate. For example, we provide SEAFaIR parameters tuned to a set of CMIP6 models, which should provide a thermal response more similar to MAGICC6 than the default. We argue that the high level of flexibility afforded by the simple thermal response model in SEAFaIR reduces the need for multiple simple models, given its surprisingly good ability to emulate a range of more complex models Tsutsui (2017).

Emulating CMIP6 models with SEAFaIR

Following Tsutsui (2017), we tune both the CO_2 concentration-forcing relation and the thermal response model to available output from the CMIP6 (Eyring et al., 2016) 1pctCO2 and abrupt-4×CO2 experiments. As in Tsutsui, we tune both two- and three-timescale variants of the thermal response model. We tune our three-term concentration-forcing equation to the variable logarithmic – quadratic relationship from Tsutsui, which changes functional form once the CO_2 concentration is over twice the pre-industrial value. We find that our equation is sufficient to well represent this variable relationship as shown in SI figure 3. The tuned parameters are given below for the 17 CMIP6 models with the required

output available.

Table 3: Default parameter values for the CO_2 concentration-forcing parameters and thermal response parameters for emulation of CMIP6 models with SEAFaIR. The f parameters are the same for both the two- and three-timescale variants.

CMIP6 model	Parameter timescales	f_1	f_2	f_3	d_1	d_2	d_3	q_1	q_2	q_3
BCC-CSM2-MR	2	6.415	0.005	-0.435	157.604	3.668	-	0.425	0.552	-
	3	-	-	-	170.678	7.421	0.707	0.379	0.331	0.23
BCC-ESM1	2	3.278	0.002	-0.001	193.231	4.188	-	0.48	0.591	-
	3	-	-	-	263.482	15.857	1.988	0.41	0.259	0.391
CESM2	2	14.385	0.027	-2.14	197.239	4.033	-	0.912	0.648	-
	3	-	-	-	212.316	6.079	0.942	0.941	0.475	0.201
CESM2-WACCM	2	2.584	0.004	-0.003	214.216	3.887	-	0.801	0.611	-
	3	-	-	-	219.713	4.775	0.279	0.801	0.524	0.095
CNRM-CM6-1	2	12.962	0.022	-1.732	282.876	4.571	-	0.685	0.707	-
	3	-	-	-	454.774	17.378	1.409	0.558	0.368	0.417
CNRM-ESM2-1	2	2.549	0.003	-0.002	338.245	5.905	-	0.817	0.776	-
	3	-	-	-	355.29	8.676	0.34	0.727	0.584	0.189
CanESM5	2	10.095	0.014	-1.081	231.427	6.235	-	0.788	0.769	-
	3	-	-	-	290.57	13.34	1.038	0.708	0.526	0.306
GFDL-CM4	2	7.719	0.009	-0.683	197.746	2.761	-	0.591	0.613	-
	3	-	-	-	223.729	6.994	0.98	0.592	0.301	0.347
GISS-E2-1-G	2	4.913	0.0	-0.0	334.568	2.561	-	0.308	0.481	-
	3	-	-	-	341.044	4.517	0.497	0.258	0.272	0.186
GISS-E2-1-H	2	4.633	0.001	0.0	181.44	3.693	-	0.38	0.533	-
	3	-	-	-	210.002	8.513	0.725	0.333	0.308	0.241
HadGEM3-GC31-LL	2	9.892	0.013	-1.05	203.002	6.345	-	0.779	0.739	-
	3	-	-	-	388.248	23.441	2.115	0.656	0.503	0.428
IPSL-CM6A-LR	2	13.65	0.024	-1.923	175.721	5.639	-	0.572	0.731	-
	3	-	-	-	228.387	13.099	0.868	0.481	0.48	0.31
MIROC-ES2L	2	10.883	0.015	-1.232	409.739	4.421	-	0.269	0.485	-
	3	-	-	-	591.245	9.721	0.925	0.205	0.26	0.212
MIROC6	2	3.884	0.002	0.0	315.851	3.121	-	0.282	0.48	-
	3	-	-	-	495.06	12.253	1.37	0.23	0.18	0.315
MRI-ESM2-0	2	10.552	0.016	-1.277	200.946	3.072	-	0.472	0.488	-
	3	-	-	-	202.58	4.503	0.385	0.447	0.346	0.14
SAM0-UNICON	2	5.201	0.0	0.0	260.591	3.396	-	0.478	0.57	-
	3	-	-	-	261.811	4.005	0.353	0.465	0.487	0.081
UKESM1-0-LL	2	5.283	-0.0	0.0	212.814	5.46	-	0.74	0.729	-
	3	-	-	-	323.251	17.44	1.265	0.634	0.461	0.381

At the time of writing, the required Earth System Model (ESM) output from CMIP6 for tuning the gas cycles is not available, however, this is something we aim to complete in the future, such as to be able to fully emulate the CMIP6 ESM ensemble for CO_2, CH_4 and N_2O.

5 SEAFaIR: RCP and SSP simulations

In this section we run several standard "benchmark" tests that have been carried out by previous simple modelling groups. These include simple pulse experiments such as in Joos et al. (2013), running both the standard RCP concentrations backwards and the corresponding but not fully compatible due to their parallel development (Moss et al., 2010) emission scenarios forwards through SEAFaIR, and comparing simulations of the more recent SSPs (Riahi et al., 2017) from other simple models used in SR15 (Huppmann et al., 2018; IPCC, 2018) with that from SEAFaIR.

Idealised Experiments

First, we run a series of standard pulse experiments. SEAFaIR is spun up to present-day (2019) with inverse emissions derived from historical concentrations (Meinshausen et al., 2017), then concentrations of CO_2, CH_4 and N_2O are fixed at 407.9 ppm, 1867 ppb and 330.8 ppb respectively; updating and approximately replicating the experimental protocol of Joos et al. (2013). All other forcings are fixed at the 2019 value. One run is carried out with no additional emissions, and the other three have an emission pulse of 1Mt of one of the gases added in 2019. A 1Mt pulse is used since unlike in the majority of models in Joos et al. (2013), SEAFaIR has no internal variability, so we do not require a pulse as large as 100Gt to obatin sufficient signal; regardless, the results obtained are independent of the pulse size over several orders of magnitude (for N_2O and CH_4 at least until the equations begin to break down due to, for example, lifetime feedbacks causing unphysical negative lifetimes). We derive four metrics for each gas: the instantaneous airbourne fraction after 100 years (IRF_{100}) – the proportion of CO_2 from the inital pulse remaining in the atmosphere; the integrated Impulse Response Function after 100 years ($iIRF_{100}$) – the integral of the instantaneous airborne fraction over the 100 years following the initial pulse; the Absolute Global Warming Potential (AGWP) – the integrated radiative forcing over a specified number of years following the pulse, normalized per kg of gas; the Global Warming Potential (GWP) after 20 and 100 years – a very widely used metric of the potency of a GHG equal to the AGWP of the GHG divided by the AGWP of CO_2 over the given time period; and the initial pulse-adjustment timescale (IPT) – the time between the inital pulse and peak warming. Both CH_4 and N_2O also contribute indirectly to radiative forcing through their atmospheric chemistry, hence GWP values are given for direct-only forcings and full forcings, for N_2O taking the absolute differences as calculated

in Myhre et al. (2013), and for CH_4 using the alternative CH_4 f_2 parameter including indirect forcings. We find values comparable to the current literature (Joos et al., 2013; Ricke and Caldeira, 2014). The full CH_4 GWP is higher than previous studies (Myhre et al., 2013; Holmes et al., 2013; Etminan et al., 2016), since we have included both the effects of a longer CH_4 lifetime as in Holmes et al. (2013) and the upwards-revised radiative forcing from Etminan et al. (2016). Our calculated IPT value for CO_2 agrees well with Zickfeld and Herrington (2015); Ricke and Caldeira (2014), however we find that while the IPT does increase with the pulse size, it does not to the extent in Zickfeld and Herrington; only by 2 – 5 years for a pulse of 1000GtC. While most metrics given below do not change significantly if calculated with a more "realistic" baseline scenario, the $iIRF_1 00$ and instantaneous airborne fraction for CO_2 do, thus we also give values for these metrics under an RCP4.5 baseline (the diagnosed inverse emissions that return the RCP database concentrations when run through SEAFaIR).

Table 4: Gas metric values from present-day pulse experiments. Uncertainties are provided as 5-95% ranges.

Metric	CO_2	CH_4	N_2O
$iIRF_{100}$ (yr)	48.4 [44.8 , 54.0]	11.8 [10.7 , 13.6]	67.3 ± 0.15
$iIRF_{100}$ (yr) – RCP4.5	55.5 [51.0 , 63.1]	11.6 [10.5 , 13.2]	67.4 ± 0.2
IRF_{100} (%)	41.6 [38.4 , 46.4]	0.0 ± 0.0	42.4 ± 0.25
IRF_{100} (%) – RCP4.5	51.8 [46.8 , 60.5]	0.0 ± 0.0	41.9 ± 0.4
$AGWP_{100}$ (10^{-13} W m^{-2} yr kg^{-1})	0.833 [0.787 , 0.906]	18.2 [16.8 , 20.3]	2.60 ± 0.06
GWP_{100} (direct-only)	1.0 ± 0.0	21.9 [19.1 , 25.3]	312 [287 , 330]
GWP_{100} (full)	1.0 ± 0.0	40.8 [35.3 , 47.8]	291 [266 , 309]
$AGWP_{20}$ (10^{-13} W m^{-2} yr kg^{-1})	0.216 [0.206 , 0.230]	15.0 [14.3 , 15.7]	71.4 ± 0.0
GWP_{20} (direct-only)	1.0 ± 0.0	69.2 [63.5 , 75.5]	330 [311 , 347]
GWP_{20} (full)	1.0 ± 0.0	129.9 [118.2 , 143.4]	309 [290 , 326]
IPT (years)	11.9 [6.9 , >100]	6.9 [5.1 , 8.4]	17.0 [11.8 , 23.9]

We also diagnose the Transient Response to Cumulative Carbon Emissions (TCRE) within SEAFaIR. This is the emergent linear relationship between global temperature anomalies and cumulative CO_2 emissions, attributed to a balance between the increasing airborne CO_2 fraction as atmospheric concentrations are raised and the approximately logarithmic concentration-forcing relationship for CO_2. Here it is calculated in two ways: once following Smith et al., in which the temperature anomaly at 1000GtC was calculated when RCP8.5 was simulated by FaIR v1.3 (here we carry out this method using RCP4.5, 6 and 8.5, running SEAFaIR with concentrations and diagnosing both inverse CO_2 emissions and temperature anomalies). This method allows both the CO_2-only TCRE and effective-TCRE (when

all forcing agents are included in the temperature response) to be determined. The effective-TCRE is not a strict relationship (unlike the CO_2-only TCRE), and depends considerably on the non-CO_2 forcing pathway taken. For this reason, the effective-TCRE varies considerably between RCPs. The second method used to diagnose the TCRE (CO_2-only) follows Gillett et al. (2013), in which we prescribe a 1% per year increase in CO_2 concentrations starting from pre-industrial levels, and determine the ratio of global-mean warming to cumulative CO_2 emissions at the point of CO_2 concentration doubling. The results are summarised in the table below. The result using the RCP 8.5 scenario is very similar to FaIR v1.3, though with slightly lowered 5 and 95% percentile, and is within the AR5 assessed range (Collins et al., 2013). The 1% experiment result of is consistent with a recent study (Millar and Friedlingstein, 2018) that utilised both the historic record and ESMs, though our result lowers the upper end of the TCRE distribution. The best-estimate effective TCRE in Millar and Friedlingstein is around 0.2°C higher than in SEAFaIR, but the range calculated here fully encapsulates the range given in that study.

Table 5: Diagnosed TCRE in SEAFaIR.

Method	Result
Effective-TCRE	
RCP8.5	1.68 [1.11 , 2.68]
RCP6	1.57 [1.03 , 2.49]
RCP4.5	1.60 [1.06 , 2.56]
CO_2-only TCRE	
RCP8.5	1.38 [0.85 , 2.14]
RCP6	1.37 [0.84 , 2.13]
RCP4.5	1.37 [0.85 , 2.11]
1% experiment	1.32 [0.80 , 2.26]

RCP simulations

Since the RCPs themselves are *concentration* pathways, here we focus on the results of running SEAFaIR with concentrations from the RCP database, as was done in the GCMs in CMIP5. We include emissions-driven runs in the Supplementary Information, but these are not comparable due to the lack of full integration between RCP concentrations and emissions as was planned in Moss et al. (2010). Figure 2 shows diagnosed emissions that are compatible with the RCP concentration series in FaIRv2.0, run with default parameters plus uncertainties as described above. Here we see the large discrepancies between SEAFaIR compatible emissions and the RCP database emissions for CH_4 and N_2O, while FaIRv2.0

diagnosed emissions agree well with bottom-up emission estimates to the present-day as expected, since SEAFaIR is tuned against a very similar historical concentration series.

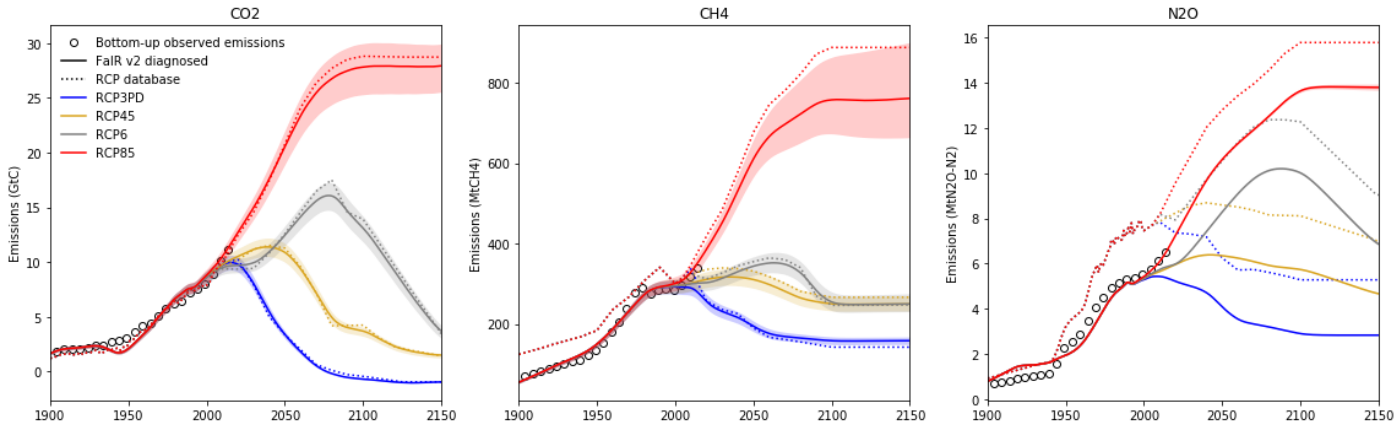

Figure 3: Diagnosed emissions corresponding to the RCPs. Solid lines show best-estimate SEAFaIR diagnosed inverse emissions, with associated 5-95% plumes. Dotted lines show emissions directly from the RCP database. Unfilled black circles show bottom-up emission estimates from GCP and PRIMAP-histTP (Quéré et al., 2018; Gütschow et al., 2016), smoothed with a 5-yearly running mean.

Figure 3 shows the corresponding radiative forcings compared to those from the RCP database. The updated simple RF formulae described in Etminan et al. (2016) increase the RF of CH_4 and CO_2, while marginally decreasing the N_2O RF.

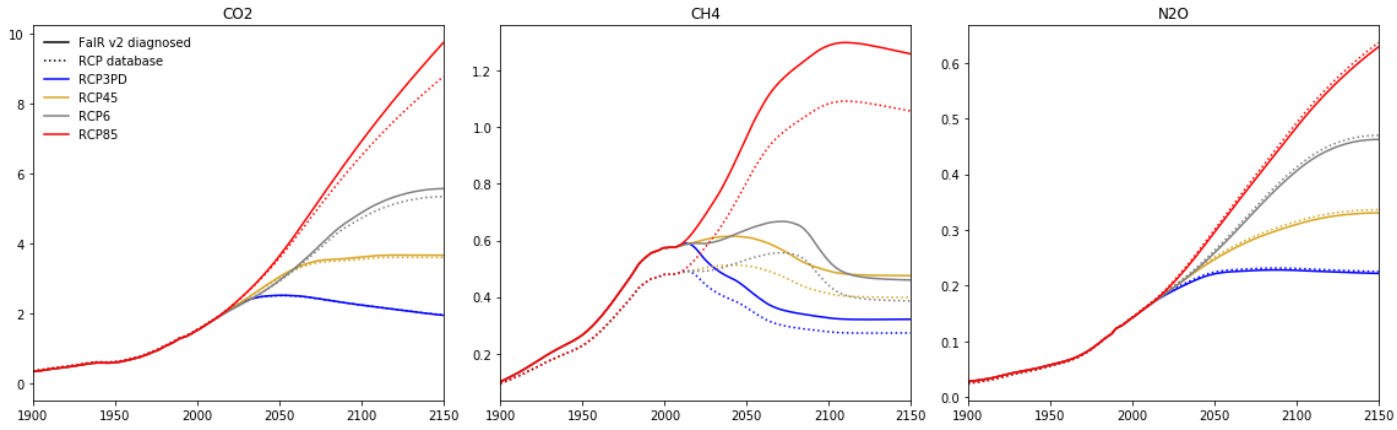

Figure 4: Simulated RCP forcing.

Figure 4 shows historical and future global mean surface temperature ranges (GMST) under the

RCP scenarios diagnosed by SEAFaIR, alongside historical observed data and future projections from CMIP5. We see that the SEAFaIR diagnosed temperatures closely resemble the observed GMST series, but are lower than the CMIP5 ranges. This is due to the default climate response parameter selection in SEAFaIR as described above and is discussed fully in Richardson et al. (2016). If instead we use CMIP5 model tuned parameters from Tsutsui (2017), we find that the resulting SEAFaIR temperatures much more closely resemble the CMIP5 ranges as seen in SI Figure 5, but still do not capture the full model spread for low forcing scenarios such as RCP3PD.

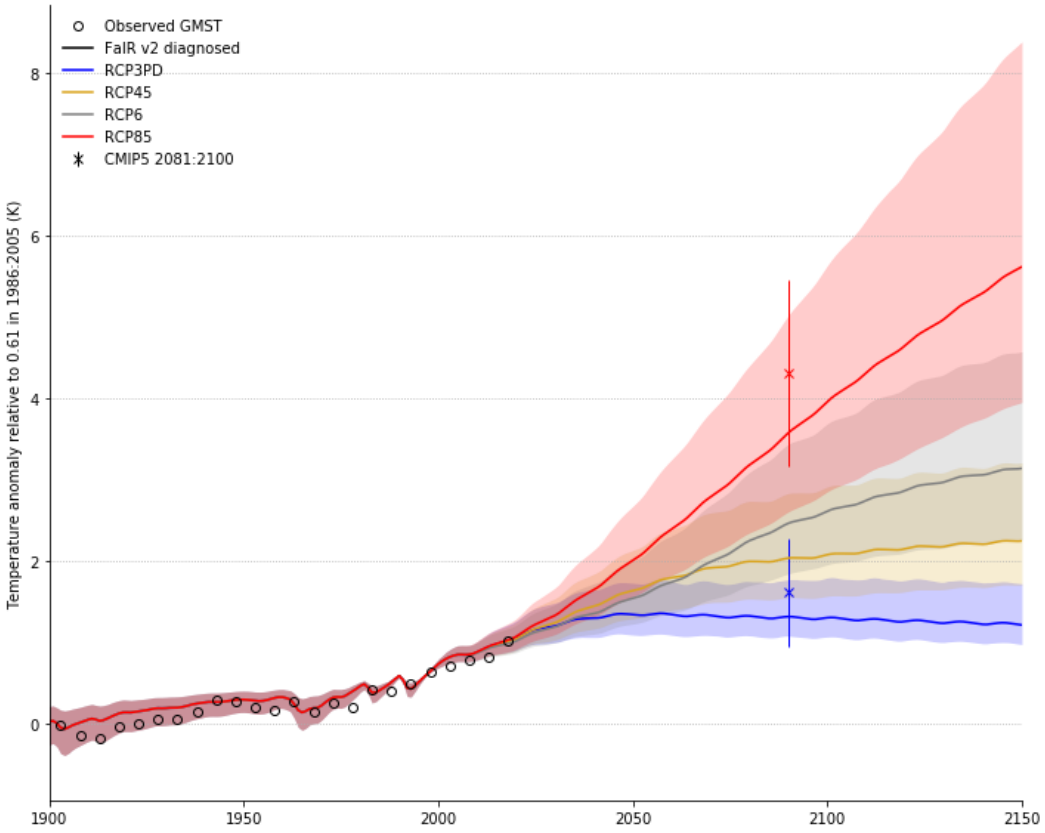

Figure 5: Simulated RCP temperature anomaly. Solid lines and plumes show best-estimate and 5-95% range temperature anomaly simulated in SEAFaIR. Unfilled black circles show observed GMST as the mean of 4 temperature datasets (Vose et al., 2012; Cowtan and Way, 2014; Lenssen et al., 2019; Morice et al., 2011), smoothed with a 5-yearly running mean. Error bars in 2090 show CMIP5 projected 2081:2100 mean temperature anomalies (Collins et al., 2013).

SSP simulations and SR15 SCM comparison

Although we include RCP simulations with SEAFaIR to allow comparison with the majority of the literature used, they have now been superceeded by the SSP scenarios used in SR15 (Riahi et al., 2017; IPCC, 2018). Here we explore emission-driven simulations of three of the SSPs from the IMAGE 3.0.1 integrated assessment model: SSP1-19, SSP2-45 and SSP5-Baseline. These three pathways span the range of possible future emissions and corresponding climates. Since the emissions series provided in the IAMC 1.5C database (Huppmann et al., 2018) only begin in 2005, we must harmonize these to historical series to spin up SEAFaIR. We do this by diagnosing historical emissions for CO_2, CH_4 and N_2O from the CMIP6 historical concentrations (Meinshausen et al., 2017) between 1750 and 2015 in SEAFaIR, then joining these to each SSP scenario in 2015, multiplying the SSP scenario by a linearly time dependent scaling factor – such that the SSP scenario emissions are equal to the diagnosed emissions in 2015 – that reaches a value of 1 by 2025. All other SSP forcings are harmonized identically, using best-estimate historical forcings from Forster et al. (2013). While this harmonization procedure does not exactly match the one used in the database scenarios, present-day CO_2 concentrations and total forcing is similar, and this hsould therefore be a representative comparison. The SEAFaIR simulated concentrations are shown in figure 5. Concentration data from other SCMs (FaIR v1.3 and MAGICC6) is only available for CO_2. We see that SEAFaIR simulates slightly lower CO_2 concentrations that the other SCMs, but that they generally lie within the 5-95% ranges. The small N_2O spread is due to its long lifetime and single atmospheric sink as modelled in SEAFaIR.

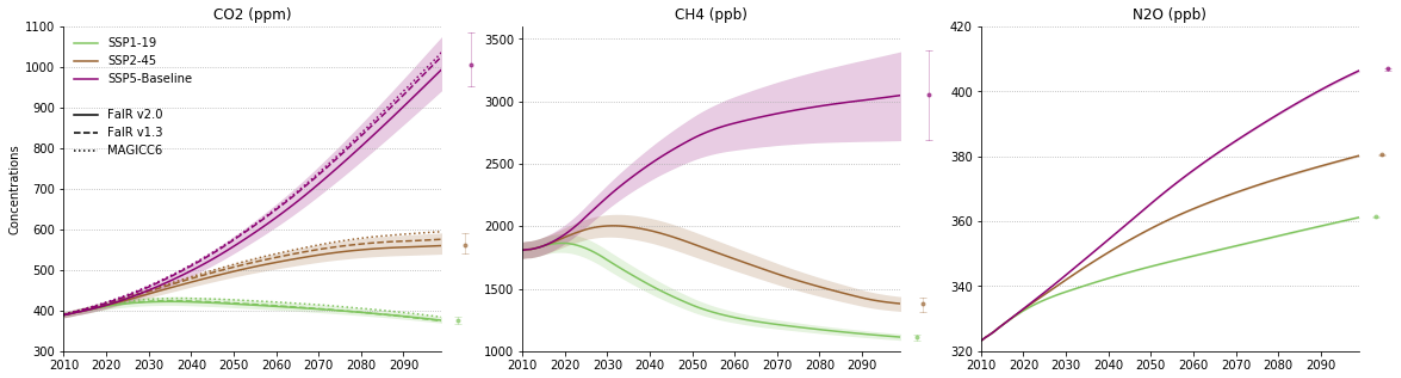

Figure 6: CO_2, CH_4 and N_2O concentrations for a range of SSP scenarios. Solid lines show concentrations simulated in SEAFaIR from harmonized emissions data as described above. Dashed lines show CO_2 concentrations in FaIR v1.3; and dotted lines show concentrations in MAGICC6, from Huppmann et al. (2018).

Median radiative forcing for each gas is available for both FaIR v1.3 and MAGICC6 in the IAMC database, so here we may do a more complete comparison between the three SCMs. Figure 6 shows that SEAFaIR has very similar CO_2 forcing to the other SCMs over the 21st century, lying between them for SSP5-Baseline and SSP1-19, and slightly below for SSP2-45. The other two SCMs lie within the SEAFaIR 5-95% ranges for all time. The CH_4 forcing highlights the difference in the CH_4 concentration-forcing relationship between the models. Both SEAFaIR and FaIR v1.3 are based on the more recent study by Etminan et al. (2016), which revised present-day CH_4 forcing upwards by 25%, while MAGICC6 is based on Myhre et al. (2013). The difference between SEAFaIR and v1.3 is largely due to the different gas cycles: SEAFaIR has an interactive CH_4 lifetime which is longer at the present-day by default, while FaIR v1.3 keeps the CH_4 lifetime constant at 9.3 years throughout (Smith et al., 2017). SEAFaIR displays very similar N_2O forcing to MAGICC6, while FaIR v1.3 lies somewhat below. This discrepancy lies with the N_2O gas cycle in FaIR v1.3, since the concentration-forcing relations in FaIR v1.3 and v2.0 are extremely similar, and is likely due to its relatively low estimate of natural N_2O emissions at the present-day of 9.1 $MtN_2O\text{-}N_2$ (the value at which future natural emissions are fixed at). This value is taken from Prather et al. (2012), but a constant lifetime of 121 years is used, rather than the present-day lifetime estimate from that study of 131 years. This combination of low lifetime and natural emission estimate is likely the cause of the lowered future concentrations and corresponding forcing. The evolution of total forcing in each scenario is highly comparable between the models, with

SEAFaIR lying marginally above the other two for the SSP5-Baseline scenario – due to its higher CH_4 forcing – and in between for the two lower emission scenarios.

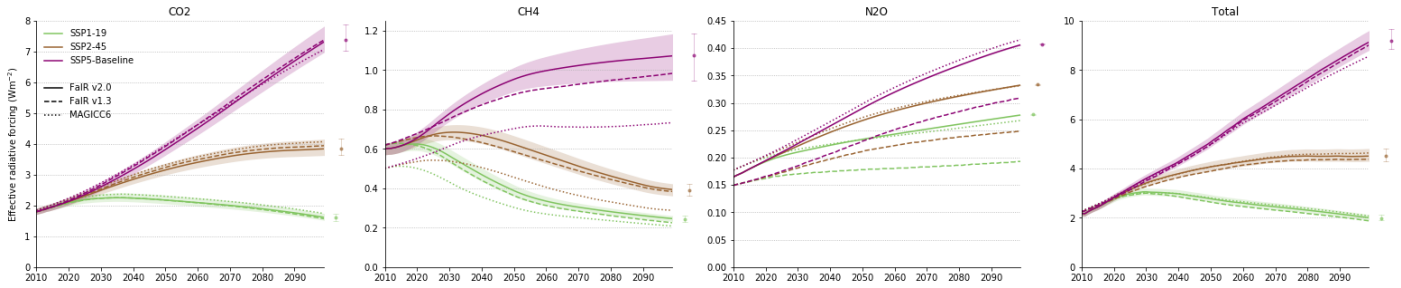

Figure 7: CO_2, CH_4 and N_2O effective radiative forcing for a range of SSP scenarios. Solid lines show ERF simulated in SEAFaIR from harmonized emissions data as described above. Dashed lines show ERF in FaIR v1.3; and dotted lines show concentrations in MAGICC6, from Huppmann et al. (2018).

Finally, we compare the probabilistic temperature anomaly in each model. Figure 7 shows the median and 5-95% temperature response (min/max for CMIP6 SEAFaIR) in default SEAFaIR, FaIR v1.3, MAGICC6, and SEAFaIR tuned to 17 CMIP6 models (two-timescale thermal response, parameters in table 3). Both SEAFaIR responses are relative to an anomaly of 0.61K in 1986:2005 (Kirtman et al., 2013), and the FaIR v1.3 and MAGICC6 responses are taken directly from the database (median 2010 anomalies are 0.95, 0.86, 0.89 and 1.09 in SEAFaIR, v1.3, MAGICC6 and CMIP6 SEAFaIR respectively). We see that the default SEAFaIR response is very similar, if marginally higher than the response of FaIR v1.3. Both versions of FaIR under default parameters have a significantly lower median response than MAGICC6, as well as a lower 5-95% spread for all scenarios. The CMIP6-tuned SEAFaIR has a higher response and lower spread than MAGICC6 for all scenarios, demonstrating the importance of thermal parameter choice in SCMs, since this is fundamentally the same model as default SEAFaIR, but has a very different response.

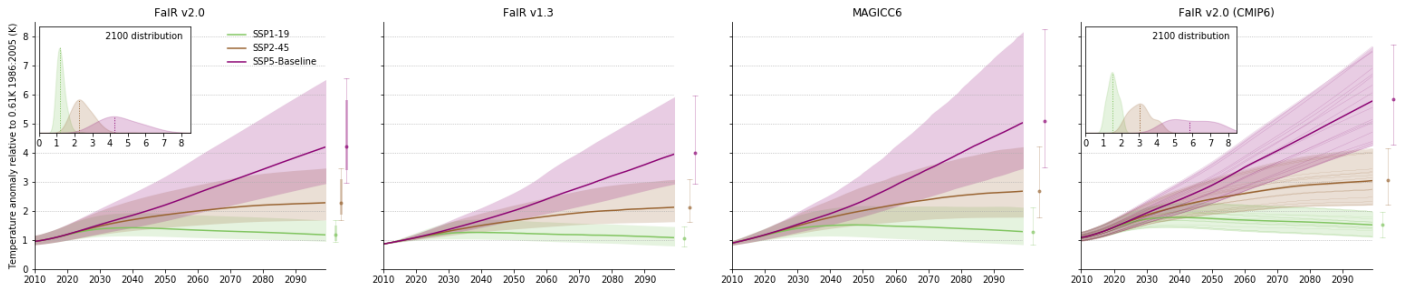

Figure 8: Temperature anomaly projections for a range of SSPs. Solid lines and plumes show median and 5-95% ranges for each model. Inset axes for SEAFaIR simulations show distribution of temperatures in 2100.

6 Use of SEAFaIR

We envisage that SEAFaIR will primarily be used for similar assessments as are carried out with the current SCMs, such as providing probabilistic projections of atmospheric concentrations, radiative forcings and temperature anomalies for wide ranges of scenarios, such as was carried out to provide the SR15 scenario explorer (Huppmann et al., 2018). SEAFaIR could also easily be coupled to integrated assessment models (IAMs) to explore impacts of climate policy options. One advantage that SEAFaIR has over the other SCMs discussed here, MAGICC6 (which is already used in several IAMs) and FaIR v1.3, is its relative computational efficiency and simple equation set. Due to its parallel treatment of all the gas species, when written in a programming language designed for array operations (such as Fortran, MATLAB, or the NumPy Python module), SEAFaIR is extremely quick to run. For example, using its current Python code, SEAFaIR can compute a full emission $\rightarrow$ concentration $\rightarrow$ radiative forcing $\rightarrow$ temperature pathways for 23 $\times$ 350 year scenarios $\times$ 3 gases (plus external forcings) $\times$ 100 gas cycle parameter sets $\times$ 200 thermal response parameter sets in just over 90 seconds[1] – around 2 million years of earth-system emulation per second. This speed provides significant advantages when computing large probabilistic ensembles, or when optimizing parameters dependent on the climate system as is done in IAMs.

The six simple equations used by SEAFaIR also provide advantages for integration into IAMs, as rather

[1]on a laptop with 31GB RAM and an Intel(R) Core(TM) i7-8750H@2.2GHz

than having to integrate the original SCM code into an existing architecture, the FaIR equations set could be written up using a language and format consistent with the IAM codebase with limited effort. Their simplicity means that SEAFaIR can be run in programs for analysis of tabular data, including (but not limited to) Excel. This opens up climate system exploration to a large group of potential new users who are familiar with spreadsheets, but not formal scientific programming languages. Finally, their simplicity adds considerably to the overall transparency of SEAFaIR; if it displays unexpected behaviour, it is easy to determine where exactly this behaviour originates and explain it.

We suggest that the speed, simplicity and transparency of SEAFaIR lends it to use in undergraduate and high-school education in addition to scientific research. It can be used to explain (and demonstrate) various aspects of both the carbon (or methane / nitrous oxide) cycle and Earth's thermal response to radiative forcing, and is simple enough to use that students could themselves carry out experiments (such as a CO_2 doubling) easily without prior experience and only basic computing skills.

The final potential use case that these authors can think of is to use SEAFaIR to explain differences between ESMs more simply through tuning SEAFaIR to emulate the ESMs and comparing differences between the tuned parameter sets to identify which aspects of the models differ most. The ability to tune SEAFaIR (Tsutsui, 2017; Joos et al., 2013; Millar et al., 2017) to more complex models also allows estimation of complex model response to a particular scenario or experiment without having to expend computer power to run SEAFaIR itself; which itself could allow climate system uncertainties to be introduced more fully into integrated assessment studies by emulating the full CMIP6 ensemble within IAMs.

7 Conclusions

In this paper we have presented a simple gas-cycle impulse-response model. This represents a significant modification to the FaIR v1.0 SCM, removing the requirement for a non-linear equation to be numerical solved with an analytic approximation, and adding a term in the state-dependence that de-

pends on the atmospheric mass burden of the gas hence allowing CH_4 and N_2O to be modelled by the same equations as CO_2. This state-dependence allows important properties of CH_4 atmospheric chemistry to be included, such as the self-feedback and the climate feedbacks from changes in tropospheric air temperatures and water vapour mixing ratio on its lifetime; and the self-feedback from N_2O on its own lifetime. Inclusion of these physically justified feedbacks should provide a more accurate emission-concentration relationship, particularly for scenarios in which feedbacks are significant such as high-emission scenarios, than models using a constant lifetime. The default gas-cycle parameters are tuned based on best-estimate observations of atmospheric concentrations and bottom-up emission estimates (Meinshausen et al., 2017; Gütschow et al., 2016), or derived from literature (Prather et al., 2015; Holmes et al., 2013; Joos et al., 2013). We use a generalised equation to model the concentration-forcing relationships of CO_2, CH_4 and N_2O, demonstrating that with the calculated default parameters we can reproduce the equations derived from spectral measurements in Etminan et al. (2016). However, as we want to maintain direct independence of each gas species, we fix the interaction terms in the Etminan et al. (2016) equations at the present-day value. This does not affect results significantly except for scenarios with extreme-high emissions of CH_4, such as RCP8.5. The thermal response model is identical to that investigated in many previous studies (Millar et al., 2017; Smith et al., 2017; Good et al., 2011; Geoffroy et al., 2013b,a; Tsutsui, 2017), so we do not focus on this component of SEAFaIR. However, we do recommend that users of SEAFaIR take care when tuning or selecting the parameters used in the thermal response component, as this has been a historically contentious issue when comparing the results of different SCMs. As such, we state here that SEAFaIR itself has neither a high nor a low response, since this is dependent entirely on the parameters chosen. We give default parameters consistent with the assessed quantities in AR5 (Myhre et al., 2013), but other parameter choices would be equally valid.

We find that we are able to reproduce atmospheric concentrations from bottom-up emission estimates accurately, without the need for specifying time-dependent natural emissions (which have very high associated uncertainties). Some discrepancies between observed concentrations and emissions estimates cannot be explained by SEAFaIR, most notably pre-1980 N_2O concentrations, but this is due to the chosen emission estimate, and future research may reconcile the two. Calculations of standard gas-cycle

model comparison metrics agree well with values from the literature using methods following Joos et al. (2013). Most notably, we find that the GWP of CH_4 is increased to 40.8 [35.3 , 47.8], due to compounding increases in both its lifetime and radiative forcing impact (Etminan et al., 2016; Holmes et al., 2013). We find policy significant differences in the timing of peak warming following pulses of CO_2, CH_4 and N_2O: a pulse of N_2O will cause a peak in attributed warming approximately 10 years after a pulse of CH_4 of equal size. SEAFaIR calculates a TCRE of 1.32 [0.80 , 2.26], very similar to previous estimates (Millar and Friedlingstein, 2018).

A comparison of simulations of selected SSPs within SEAFaIR against other widely used SCMs, FaIR v1.3 and MAGICC6, highlights differences between the three models. These can all be explained by parameter selection in each model, and is caused by differences in the studies or data sources which each model has been tuned to reproduce; such as the concentration-forcing relationships in MAGICC6 following the simple relations in Myhre et al. (2013) while in FaIR v1.3 and this model they follow the updated relations in Etminan et al. (2016). Crucially, we demonstrate that differences between the thermal response in these models is entirely dependent on the parameter selection, demonstrating this using two different parameter sets within our single model: one tuned to individual GCMs in the CMIP6 ensemble (Tsutsui, 2017), and one using the assessed range in AR5 (Collins et al., 2013).

There are many potential uses for SEAFaIR as a result of its simplicity and transparency. In addition to being used for the same probabilistic scenario assessment as is carried out by SCMs in reports such as SR15 (IPCC, 2018), it could be very easily implemented into IAMs; and may provide some improvements in terms of computational efficiency due to its extremely rapid runtime. We also encourage SEAFaIR to be used by policy-makers in order to directly assess whether the warming implications are aligned with the intended outcomes of mitigation policies; since GHG accounting metrics used at present such as GWP do not provide accurate results for targets such as Net-Zero CO_2 due to the short life of some GHGs (Allen et al., 2018). To promote this sort of use of SEAFaIR, we provide an Excel file containing the model with its default parameter set to give access to SEAFaIR for users unfamiliar with scientific programming languages. This version of the model could also be used to aid teaching of climate change and climate processes; and could even allow students access to an easy-to-understand

model that they could use themselves to explore future scenarios and the relative impacts of future emissions of CO_2, CH_4 and N_2O; or the importance of climate sensitivity.

We aim to be able to provide gas-cycle parameter sets tuned to each of the CMIP6 ESMs in the near future, such that SEAFaIR could be used to emulate the full CMIP6 ensemble. These parameter sets could also be used to improve understanding of how these models differ in a single consistent framework. Combining implementation of SEAFaIR into IAMs with these parameter sets would allow uncertainty in climate models to be included in socio-economic projections dependent on future climate in a more consistent manner to the uncertainties in pure climate model projections than using SCMs with their default parameter sets and uncertainties.

References

Allen, M. R., Frame, D. J., Huntingford, C., Jones, C. D., Lowe, J. A., Meinshausen, M., and Meinshausen, N. (2009). Warming caused by cumulative carbon emissions towards the trillionth tonne. *Nature*, 458(7242):1163–1166.

Allen, M. R., Shine, K. P., Fuglestvedt, J. S., Millar, R. J., Cain, M., Frame, D. J., and Macey, A. H. (2018). A solution to the misrepresentations of CO2-equivalent emissions of short-lived climate pollutants under ambitious mitigation. *npj Climate and Atmospheric Science*, 1(1).

Arora, V. K., Melton, J. R., and Plummer, D. (2018). An assessment of natural methane fluxes simulated by the CLASS-CTEM model. *Biogeosciences*, 15:4683–4709.

Battle, M., Bender, M., Sowers, T., Tans, P. P., Butler, J. H., Elkins, J. W., Ellis, J. T., Conway, T., Zhang, N., Lang, P., and Clarket, A. D. (1996). Atmospheric gas concentrations over the past century measured in air from firn at the South Pole. *Nature*, 383(6597):231–235.

Butler, J. H., Battle, M., Bender, M. L., Montzka, S. A., Clarke, A. D., Saltzman, E. S., Sucher, C. M., Severinghaus, J. P., and Elkins, J. W. (1999). A record of atmospheric halocarbons during the twentieth century from polar firn air. *Nature*, 399(6738):749–755.

Collins, M., Knutti, R., Arblaster, J., Dufresne, J.-L., Fichefet, T., Friedlingstein, P., Gao, X., Gutowski, W. J., Johns, T., Krinner, G., Shongwe, M., Tebaldi, C., Weaver, A. J., and Wehner, M. (2013). Long-term Climate Change: Projections, Commitments and Irreversibility. In Stocker, T. F., Qin, D., Plattner, G.-K., Tignor, M., Allen, S. K., Boschung, J., Nauels, A., Xia, Y., Bex, V., and Midgley, P. M., editors, *Climate Change 2013: The Physical Science Basis. Contribution of Working Group I to the Fifth Assessment Report of the Intergovernmental Panel on Climate Change*, chapter 12, pages 1029–1136. Cambridge University Press, Cambridge, United Kingdom and New York, NY, USA.

Cowtan, K. and Way, R. G. (2014). Coverage bias in the HadCRUT4 temperature series and its impact on recent temperature trends. *Quarterly Journal of the Royal Meteorological Society*, 140(683):1935–1944.

Cunnold, D. M., Fraser, P. J., Weiss, R. F., Prinn, R. G., Simmonds, P. G., Miller, B. R., Alyea, F. N., and Crawford, A. J. (1994). Global trends and annual releases of CCl 3 F and CCl 2 F 2 estimated from ALE/GAGE and other measurements from July 1978 to June 1991 . *Journal of Geophysical Research*, 99(D1):1107.

Davidson, E. A. and Kanter, D. (2014). Inventories and scenarios of nitrous oxide emissions. *Environmental Research Letters*, 9(10).

Etminan, M., Myhre, G., Highwood, E. J., and Shine, K. P. (2016). Radiative forcing of carbon dioxide, methane, and nitrous oxide: A significant revision of the methane radiative forcing. *Geophysical Research Letters*, 43(24):12,614–12,623.

Eyring, V., Bony, S., Meehl, G. A., Senior, C. A., Stevens, B., Stouffer, R. J., and Taylor, K. E. (2016). Overview of the Coupled Model Intercomparison Project Phase 6 (CMIP6) experimental design and organization. *Geoscientific Model Development*, 9(5):1937–1958.

Forster, P. M., Andrews, T., Good, P., Gregory, J. M., Jackson, L. S., and Zelinka, M. (2013). Evaluating adjusted forcing and model spread for historical and future scenarios in the CMIP5 generation of climate models. *Journal of Geophysical Research: Atmospheres*, 118(3):1139–1150.

Geoffroy, O., Saint-Martin, D., Bellon, G., Voldoire, A., Olivié, D. J. L., Tytéca, S., Geoffroy, O., Saint-Martin, D., Bellon, G., Voldoire, A., Olivié, D. J. L., and Tytéca, S. (2013a). Transient Climate

Response in a Two-Layer Energy-Balance Model. Part II: Representation of the Efficacy of Deep-Ocean Heat Uptake and Validation for CMIP5 AOGCMs. *Journal of Climate*, 26(6):1859–1876.

Geoffroy, O., Saint-Martin, D., Olivié, D. J. L., Voldoire, A., Bellon, G., Tytéca, S., Geoffroy, O., Saint-Martin, D., Olivié, D. J. L., Voldoire, A., Bellon, G., and Tytéca, S. (2013b). Transient Climate Response in a Two-Layer Energy-Balance Model. Part I: Analytical Solution and Parameter Calibration Using CMIP5 AOGCM Experiments. *Journal of Climate*, 26(6):1841–1857.

Gillett, N. P., Arora, V. K., Matthews, D., Allen, M. R., Gillett, N. P., Arora, V. K., Matthews, D., and Allen, M. R. (2013). Constraining the Ratio of Global Warming to Cumulative CO ₂ Emissions Using CMIP5 Simulations*. *Journal of Climate*, 26(18):6844–6858.

Good, P., Gregory, J. M., and Lowe, J. A. (2011). A step-response simple climate model to reconstruct and interpret AOGCM projections. *Geophysical Research Letters*, 38(1):n/a–n/a.

Gregory, J. M., Andrews, T., and Good, P. (2015). The inconstancy of the transient climate response parameter under increasing CO ₂. *Philosophical Transactions of the Royal Society A: Mathematical, Physical and Engineering Sciences*, 373(2054):20140417.

Gütschow, J., Jeffery, M. L., Gieseke, R., Gebel, R., Stevens, D., Krapp, M., and Rocha, M. (2016). The PRIMAP-hist national historical emissions time series. *Earth System Science Data*, 8(2):571–603.

Haustein, K., Allen, M. R., Forster, P. M., Otto, F. E. L., Mitchell, D. M., Matthews, H. D., and Frame, D. J. (2017). A real-time Global Warming Index. *Scientific Reports*, 7(1):15417.

Holmes, C. D., Prather, M. J., Søvde, O. A., and Myhre, G. (2013). Future methane, hydroxyl, and their uncertainties: Key climate and emission parameters for future predictions. *Atmospheric Chemistry and Physics*, 13:285–302.

Huppmann, D., Kriegler, E., Krey, V., Riahi, K., Rogelj, J., Rose, S. K., Weyant, J., Bauer, N., Bertram, C., Bosetti, V., Calvin, K., Doelman, J., Drouet, L., Emmerling, J., Frank, S., Fujimori, S., Gernaat, D., Grubler, A., Guivarch, C., Haigh, M., Holz, C., Iyer, G., Kato, E., Keramidas, K., Kitous, A., Leblanc, F., Liu, J.-Y., Löffler, K., Luderer, G., Marcucci, A., McCollum, D., Mima, S., Popp, A., Sands, R. D., Sano, F., Strefler, J., Tsutsui, J., Van Vuuren, D., Vrontisi, Z., Wise, M., and Zhang, R.

(2018). IAMC 1.5C Scenario Explorer and Data hosted by IIASA. Integrated Assessment Modeling Consortium & International Institute for Applied Systems Analysis.

IPCC (2018). *Global warming of 1.5C. An IPCC Special Report on the impacts of global warming of 1.5C above pre-industrial levels and related global greenhouse gas emission pathways, in the context of strengthening the global response to the threat of climate change,*.

Ivy, D. J., Rigby, M., Baasandorj, M., Burkholder, J. B., and Prinn, R. G. (2012). Atmospheric Chemistry and Physics Global emission estimates and radiative impact of C 4 F 10 , C 5 F 12 , C 6 F 14 , C 7 F 16 and C 8 F 18. *Atmos. Chem. Phys*, 12:7635–7645.

Joos, F., Roth, R., Fuglestvedt, J. S., Peters, G. P., Enting, I. G., Von Bloh, W., Brovkin, V., Burke, E. J., Eby, M., Edwards, N. R., Friedrich, T., Frölicher, T. L., Halloran, P. R., Holden, P. B., Jones, C., Kleinen, T., Mackenzie, F. T., Matsumoto, K., Meinshausen, M., Plattner, G.-K., Reisinger, A., Segschneider, J., Shaffer, G., Steinacher, M., Strassmann, K., Tanaka, K., Timmermann, A., Weaver, A. J., Frölicher 11, T. L., Halloran, P. R., Holden, P. B., Jones, C., Kleinen, T., Mackenzie, F. T., Matsumoto, K., Meinshausen, M., Plattner, G.-K., Reisinger, A., Segschneider, J., Shaffer, G., Steinacher, M., Strassmann, K., Tanaka, K., Timmermann, A., and Weaver, A. J. (2013). Carbon dioxide and climate impulse response functions for the computation of greenhouse gas metrics: a multi-model analysis. *Atmos. Chem. Phys*, 13(5):2793–2825.

Kirschke, S., Bousquet, P., Ciais, P., Saunois, M., Canadell, J. G., Dlugokencky, E. J., Bergamaschi, P., Bergmann, D., Blake, D. R., Bruhwiler, L., Cameron-Smith, P., Castaldi, S., Chevallier, F., Feng, L., Fraser, A., Heimann, M., Hodson, E. L., Houweling, S., Josse, B., Fraser, P. J., Krummel, P. B., Lamarque, J. F., Langenfelds, R. L., Le Quéré, C., Naik, V., O'doherty, S., Palmer, P. I., Pison, I., Plummer, D., Poulter, B., Prinn, R. G., Rigby, M., Ringeval, B., Santini, M., Schmidt, M., Shindell, D. T., Simpson, I. J., Spahni, R., Steele, L. P., Strode, S. A., Sudo, K., Szopa, S., Van Der Werf, G. R., Voulgarakis, A., Van Weele, M., Weiss, R. F., Williams, J. E., and Zeng, G. (2013). Three decades of global methane sources and sinks.

Kirtman, B., Power, S. B., Adedoyin, J. A., Boer, G. J., Bojariu, R., Camilloni, I., Doblas-Reyes, F. J., Fiore, A. M., Kimoto, M., Meehl, G. A., Prather, M., Sarr, A., Schar, C., Sutton, R., vanOldenborgh, G. J., Vecchi, G., and Wang, H. J. (2013). Near-term Climate Change: Projections and Predictability.

In Stocker, T. F., Qin, D., Plattner, G.-K., Tignor, M., Allen, S. K., Boschung, J., Nauels, A., Xia, Y., Bex, V., and Midgley, P. M., editors, *Climate Change 2013: The Physical Science Basis. Contribution of Working Group I to the Fifth Assessment Report of the Intergovernmental Panel on Climate Change*, chapter 11, pages 953–1028. Cambridge University Press, Cambridge, United Kingdom and New York, NY, USA.

Lenssen, N. J. L., Schmidt, G. A., Hansen, J. E., Menne, M. J., Persin, A., Ruedy, R., and Zyss, D. (2019). Improvements in the uncertainty model in the Goddard Institute for Space Studies Surface Temperature (GISTEMP) analysis. *Journal of Geophysical Research: Atmospheres*, page 2018JD029522.

Meinshausen, M., Raper, S. C. B., and Wigley, T. M. L. (2011a). Emulating coupled atmosphere-ocean and carbon cycle models with a simpler model, MAGICC6 Part 1: Model description and calibration. *Atmospheric Chemistry and Physics*, 11(4):1417–1456.

Meinshausen, M., Smith, S. J., Calvin, K., Daniel, J. S., Kainuma, M. L. T., Lamarque, J.-F., Matsumoto, K., Montzka, S. A., Raper, S. C. B., Riahi, K., Thomson, A., Velders, G. J. M., and van Vuuren, D. P. (2011b). The RCP greenhouse gas concentrations and their extensions from 1765 to 2300. *Climatic Change*, 109(1-2):213–241.

Meinshausen, M., Vogel, E., Nauels, A., Lorbacher, K., Meinshausen, N., Etheridge, D. M., Fraser, P. J., Montzka, S. A., Rayner, P. J., Trudinger, C. M., Krummel, P. B., Beyerle, U., Canadell, J. G., Daniel, J. S., Enting, I. G., Law, R. M., Lunder, C. R., O'Doherty, S., Prinn, R. G., Reimann, S., Rubino, M., Velders, G. J. M., Vollmer, M. K., Wang, R. H. J., and Weiss, R. (2017). Historical greenhouse gas concentrations for climate modelling (CMIP6). *Geoscientific Model Development*, 10(5):2057–2116.

Millar, R. J. and Friedlingstein, P. (2018). The utility of the historical record for assessing the transient climate response to cumulative emissions. *Philosophical Transactions of the Royal Society of London A: Mathematical, Physical and Engineering Sciences*, 376(2119).

Millar, R. J., Nicholls, Z. R., Friedlingstein, P., and Allen, M. R. (2017). A modified impulse-response

representation of the global near-surface air temperature and atmospheric concentration response to carbon dioxide emissions. *Atmospheric Chemistry and Physics*, 17(11):7213–7228.

Millar, R. J., Otto, A., Forster, P. M., Lowe, J. A., Ingram, W. J., and Allen, M. R. (2015). Model structure in observational constraints on transient climate response. *Climatic Change*, 131(2):199–211.

Morice, C. P., Kennedy, J. J., Rayner, N. A., Jones, P. D., P., M. C., J., K. J., A., R. N., and D., J. P. (2011). Quantifying uncertainties in global and regional temperature change using an ensemble of observational estimates: The HadCRUT4 data set. *Journal of Geophysical Research: Atmospheres*, 117(D8).

Moss, R. H., Edmonds, J. A., Hibbard, K. A., Manning, M. R., Rose, S. K., Van Vuuren, D. P., Carter, T. R., Emori, S., Kainuma, M., Kram, T., Meehl, G. A., Mitchell, J. F. B., Nakicenovic, N., Riahi, K., Smith, S. J., Stouffer, R. J., Thomson, A. M., Weyant, J. P., and Wilbanks, T. J. (2010). The next generation of scenarios for climate change research and assessment. *Nature*, 463.

Myhre, G., Shindell, D., Breon, F.-M., Collins, W., Fuglestvedt, J., Huang, J., Koch, D., Lamarque, J.-F., Lee, D., Mendoza, B., Nakajima, T., Robock, A., Stephens, G., Takemura, T., and Zhang, H. (2013). Anthropogenic and Natural Radiative Forcing. In Stocker, T. F., Qin, D., Plattner, G.-K., Tignor, M., Allen, S. K., Boschung, J., Nauels, A., Xia, Y., Bex, V., and Midgley, P. M., editors, *Climate Change 2013: The Physical Science Basis. Contribution of Working Group I to the Fifth Assessment Report of the Intergovernmental Panel on Climate Change*, chapter 8, pages 659–740. Cambridge University Press, Cambridge, United Kingdom and New York, NY, USA.

Noël, S., Weigel, K., Bramstedt, K., Rozanov, A., Weber, M., Bovensmann, H., and Burrows, J. P. (2018). Water vapour and methane coupling in the stratosphere observed using SCIAMACHY solar occultation measurements. *Atmos. Chem. Phys*, 18:4463–4476.

O'doherty, S., Rigby, M., Mühle, J., Ivy, D. J., Miller, B. R., Young, D., Simmonds, P. G., Reimann, S., Vollmer, M. K., Krummel, P. B., Fraser, P. J., Steele, L. P., Dunse, B., Salameh, P. K., Harth, C. M., Arnold, T., Weiss, R. F., Kim, J., Park, S., Li, S., Lunder, C., Hermansen, O., Schmidbauer, N., Zhou, L. X., Yao, B., Wang, R. H. J., Manning, A. J., and Prinn, R. G. (2014). Global emissions

of HFC-143a (CH 3 CF 3) and HFC-32 (CH 2 F 2) from in situ and air archive atmospheric observations. *Atmos. Chem. Phys*, 14:9249–9258.

Owens, A. J., Steed, J. M., Filkin, D. L., Miller, C., and Jesson, J. P. (1982). The Potential effects of increased methane on atmospheric ozone. *Geophysical Research Letters*, 9(9):1105–1108.

Prather, M. J., Holmes, C. D., and Hsu, J. (2012). Reactive greenhouse gas scenarios: Systematic exploration of uncertainties and the role of atmospheric chemistry. *Geophysical Research Letters*.

Prather, M. J., Hsu, J., DeLuca, N. M., Jackman, C. H., Oman, L. D., Douglass, A. R., Fleming, E. L., Strahan, S. E., Steenrod, S. D., Søvde, O. A., Isaksen, I. S. A., Froidevaux, L., and Funke, B. (2015). Measuring and modeling the lifetime of nitrous oxide including its variability. *Journal of Geophysical Research: Atmospheres*, 120(11):5693–5705.

Quéré, C., Andrew, R., Friedlingstein, P., Sitch, S., Hauck, J., Pongratz, J., Pickers, P., Ivar Korsbakken, J., Peters, G., Canadell, J., Arneth, A., Arora, V., Barbero, L., Bastos, A., Bopp, L., Ciais, P., Chini, L., Ciais, P., Doney, S., Gkritzalis, T., Goll, D., Harris, I., Haverd, V., Hoffman, F., Hoppema, M., Houghton, R., Hurtt, G., Ilyina, T., Jain, A., Johannessen, T., Jones, C., Kato, E., Keeling, R., Klein Goldewijk, K., Landschützer, P., Lefèvre, N., Lienert, S., Liu, Z., Lombardozzi, D., Metzl, N., Munro, D., Nabel, J., Nakaoka, S. I., Neill, C., Olsen, A., Ono, T., Patra, P., Peregon, A., Peters, W., Peylin, P., Pfeil, B., Pierrot, D., Poulter, B., Rehder, G., Resplandy, L., Robertson, E., Rocher, M., Rödenbeck, C., Schuster, U., Skjelvan, I., Séférian, R., Skjelvan, I., Steinhoff, T., Sutton, A., Tans, P., Tian, H., Tilbrook, B., Tubiello, F., Van Der Laan-Luijkx, I., Van Der Werf, G., Viovy, N., Walker, A., Wiltshire, A., Wright, R., Zaehle, S., and Zheng, B. (2018). Global Carbon Budget 2018. *Earth System Science Data*, 10(4):2141–2194.

Riahi, K., van Vuuren, D. P., Kriegler, E., Edmonds, J., O'Neill, B. C., Fujimori, S., Bauer, N., Calvin, K., Dellink, R., Fricko, O., Lutz, W., Popp, A., Cuaresma, J. C., KC, S., Leimbach, M., Jiang, L., Kram, T., Rao, S., Emmerling, J., Ebi, K., Hasegawa, T., Havlik, P., Humpenöder, F., Da Silva, L. A., Smith, S., Stehfest, E., Bosetti, V., Eom, J., Gernaat, D., Masui, T., Rogelj, J., Strefler, J., Drouet, L., Krey, V., Luderer, G., Harmsen, M., Takahashi, K., Baumstark, L., Doelman, J. C., Kainuma, M., Klimont, Z., Marangoni, G., Lotze-Campen, H., Obersteiner, M., Tabeau, A., and

Tavoni, M. (2017). The Shared Socioeconomic Pathways and their energy, land use, and greenhouse gas emissions implications: An overview. *Global Environmental Change*, 42:153–168.

Richardson, M., Cowtan, K., Hawkins, E., and Stolpe, M. B. (2016). Reconciled climate response estimates from climate models and the energy budget of Earth. *Nature Climate Change*, 6(10):931–935.

Ricke, K. L. and Caldeira, K. (2014). Maximum warming occurs about one decade after a carbon dioxide emission. *Environmental Research Letters*, 9(12):124002.

Rigby, M., Ganesan, A. L., and Prinn, R. G. (2011). Deriving emissions time series from sparse atmospheric mole fractions. *Journal of Geophysical Research Atmospheres*, 116(8).

Saikawa, E., Prinn, R. G., Dlugokencky, E., Ishijima, K., Dutton, G. S., Hall, B. D., Langenfelds, R., Tohjima, Y., Machida, T., Manizza, M., Rigby, M., O'Doherty, S., Patra, P. K., Harth, C. M., Weiss, R. F., Krummel, P. B., Van Der Schoot, M., Fraser, P. J., Steele, L. P., Aoki, S., Nakazawa, T., and Elkins, J. W. (2014). Global and regional emissions estimates for N2O. *Atmospheric Chemistry and Physics*.

Saunois, M., Stavert, A. R., Poulter, B., Bousquet, P., Canadell, J. G., Jackson, R. B., Raymond, P. A., Dlugokencky, E. J., Houweling, S., Patra, P. K., Ciais, P., Arora, V. K., Bastviken, D., Bergamaschi, P., Blake, D. R., Brailsford, G., Carlson, K. M., Parker, R. J., Peng, C., Peng, S., Peters, G. P., Prigent, C., Prinn, R., Ramonet, M., Regnier, P., Riley, W. J., Rosentreter, J. A., Segers, A., Simpson, I. J., Shi, H., Smith, S. J., Steele, P. L., Thornton, B. F., Tian, H., Tohjima, Y., Tubiello, F. N., Tsuruta, A., Viovy, N., Voulgarakis, A., Weber, T. S., van Weele, M., van der Werf, G. R., Weiss, F., Worthy, D., Wunch, D., Yin, Y., Yoshida, Y., Zhang, W., Zhang, Z., Zhao, Y., Zheng, B., Zhu, Q., Zhu, Q., and Zhuang, Q. (2019). The Global Methane Budget 2000-2017 Earth System Science Data Discussions. *Earth System Science Data*.

Smith, C. J., Forster, P. M., Allen, M., Leach, N., Millar, R. J., Passerello, G. A., and Regayre, L. A. (2017). FAIR v1.1: A simple emissions-based impulse response and carbon cycle model. *Geoscientific Model Development Discussions*, (December):1–45.

Tian, H., Yang, J., Lu, C., Xu, R., Canadell, J. G., Jackson, R. B., Arneth, A., Chang, J., Chen, G., Ciais, P., Gerber, S., Ito, A., Huang, Y., Joos, F., Lienert, S., Messina, P., Olin, S., Pan, S., Peng, C., Saikawa, E., Thompson, R. L., Vuichard, N., Winiwarter, W., Zaehle, S., Zhang, B., Zhang, K., and Zhu, Q. (2018). The global N2O model intercomparison project. *Bulletin of the American Meteorological Society*, 99(6):1231–1251.

Tsutsui, J. (2017). Quantification of temperature response to CO2 forcing in atmosphereocean general circulation models. *Climatic Change*, 140(2):287–305.

Turner, A. J., Frankenberg, C., and Kort, E. A. (2019). Interpreting contemporary trends in atmospheric methane. *Proceedings of the National Academy of Sciences*.

Vollmer, M. K., Miller, B. R., Rigby, M., Reimann, S., Mühle, J., Krummel, P. B., O'Doherty, S., Kim, J., Rhee, T. S., Weiss, R. F., Fraser, P. J., Simmonds, P. G., Salameh, P. K., Harth, C. M., Wang, R. H., Steele, L. P., Young, D., Lunder, C. R., Hermansen, O., Ivy, D., Arnold, T., Schmidbauer, N., Kim, K. R., Greally, B. R., Hill, M., Leist, M., Wenger, A., and Prinn, R. G. (2011). Atmospheric histories and global emissions of the anthropogenic hydrofluorocarbons HFC-365mfc, HFC-245fa, HFC-227ea, and HFC-236fa. *Journal of Geophysical Research Atmospheres*.

Vose, R. S., Arndt, D., Banzon, V. F., Easterling, D. R., Gleason, B., Huang, B., Kearns, E., Lawrimore, J. H., Menne, M. J., Peterson, T. C., Reynolds, R. W., Smith, T. M., Williams, C. N., Wuertz, D. B., Vose, R. S., Arndt, D., Banzon, V. F., Easterling, D. R., Gleason, B., Huang, B., Kearns, E., Lawrimore, J. H., Menne, M. J., Peterson, T. C., Reynolds, R. W., Smith, T. M., Jr., C. N. W., and Wuertz, D. B. (2012). NOAA's Merged LandOcean Surface Temperature Analysis. *Bulletin of the American Meteorological Society*, 93(11):1677–1685.

Zickfeld, K. and Herrington, T. (2015). The time lag between a carbon dioxide emission and maximum warming increases with the size of the emission. *Environmental Research Letters*, 10(3).